RESEARCH ARTICLE | DECEMBER 20 2024

Low temperature heat transport in crystalline bismuth telluride

Remo A. Masut

AIP Advances 14, 125221 (2024)
https://doi.org/10.1063/5.0234485

Low temperature heat transport in crystalline bismuth telluride

Cite as: AIP Advances 14, 125221 (2024); doi: 10.1063/5.0234485
Submitted: 12 November 2024 • Accepted: 5 December 2024 •
Published Online: 20 December 2024

Remo A. Masut[a)]

AFFILIATIONS

Département de Génie physique, Polytechnique Montréal, CP 6079, succ. Centre-ville, Montréal, Quebec H3C 3A7, Canada

[a)]Author to whom correspondence should be addressed: remo.masut@polymtl.ca

ABSTRACT

Thermoelectric (TE) alloys based on Bi_2Te_3 are under intense development for current large-scale industrial applications. A quantitative understanding of their lattice thermal conductivity κ_{lat} is trailing mainly for two reasons: (i) lack of reliable κ_{lat} data and, surprisingly, (ii) lack of precise knowledge of the thermal properties of the parent compound, even in its crystalline form. In this work, we examine the existing data on crystalline Bi_2Te_3 and point out why data below its Debye temperature Θ_D are necessary in order to develop a better understanding of heat transfer in the compound and alloys under current development. The measured temperature dependence of κ_{lat} from 2–300 K is compared to a simplified heat transport model based on the relaxation time approximation, as well as to more recent and elaborate calculations. Most data on polycrystalline TE materials currently under development only cover a limited temperature range above their Debye temperature Θ_D. Yet, comparisons with hot extruded bulk polycrystalline Bi–Sb–Te–Se alloys with compositions close to Bi_2Te_3 stress the importance of obtaining data below Θ_D in order to advance our understanding of the thermal properties of these materials so important for TE applications below 500 K. Attempting to understand and examine the thermal transport of solids based on the approximations involved in the pioneering work of the late 1950s is not justified except below their Debye temperature.

I. INTRODUCTION

Since the mid-1950s, bismuth telluride (Bi_2Te_3) has been intensely researched as the prime thermoelectric (TE) material for refrigeration near room temperature and also for electric power generation up to ~450 K.[1] More recently, it has also surfaced as a topological insulator,[2] with its phases possibly protected even in polycrystalline form.[3] A renewed interest has risen in alloys based on Bi, Sb, Te, and Se, to improve their performance for current TE applications,[4–8] as well as in Bi_2Te_3 for more diversified applications and devices involving its TE properties.[9–12]

For these various applications, the material properties are important mostly at temperatures slightly below and above ambient, and consequently, they are characterized in that temperature range. Unfortunately, this restricted temperature range severely hinders the fundamental understanding of their thermal properties and, in particular, of their lattice thermal conductivity $\underset{\sim}{\kappa}_{lat}$, a tensor property.[13]

From a practical as well as a fundamental point of view, it is important to understand the lattice thermal conductivity in materials that are currently being considered for most wide-reaching applications of thermoelectricity. It turns out, surprisingly, that a quantitative model of the lattice thermal conductivity at low temperatures (<100 K) appears to be lacking for crystalline bismuth telluride (c-Bi_2Te_3). In order to clarify this, we first review in Sec. II the existing different theoretical approaches and experimental data on the lattice thermal conductivity of c-Bi_2Te_3. It will be evident from this limited review that the only existing data at temperatures well below the Bi_2Te_3 Debye temperature (Θ_D = 155.5 K) have been ignored in most modelization efforts. Moreover, as will be shown in Sec. II, the data gathered close to ambient temperature are not as reliable as are usually presented in the literature.

Meanwhile, there is a large body of literature that can explain the lattice thermal conductivity of solids based on the relaxation time approximation.[14–18] These approximate models can provide quantitative information on the lattice thermal conductivity of solids at temperatures lower than ~Θ_D/2, where significant changes in this property really occur. As will be shown in Sec. III, where we develop one such model based on the Debye approximation of the phonon density of states (PDOS), it is possible to fit $\underset{\sim}{\kappa}_{lat}$ quite precisely below

~100 K, the domain of its validity. This modeling can be coerced to calculate, at a given temperature T, properties such as the spectral composition of $\underset{\sim}{\kappa}_{lat}(\omega, T)$ and of the phonon mean free path $\Lambda_{ph}(\omega, T)$, yet the approach may not be entirely self-consistent. We also calculate the phonon average mean free path as a function of temperature $\langle \Lambda_{ph}(T) \rangle$ up to ~300 K. As a final cautionary note, we emphasize the need to revise the current state of the experimental determination of $\underset{\sim}{\kappa}_{lat}$ at low temperatures to provide a better understanding of this transport property. A theoretical understanding, outside of a phenomenological model based on the relaxation time approximation, will require further work.

Recent literature on the lattice thermal conductivity of polycrystalline thermoelectric alloys shows attempts to model $\underset{\sim}{\kappa}_{lat}$ using the approach developed in Refs. 14–18, usually applied to explain data taken at temperatures between 300 and 600 K, above Θ_D. Based on the results of this work, this practice should be discouraged.

II. MODELING THE LATTICE THERMAL CONDUCTIVITY OF BISMUTH TELLURIDE

Here, we gather and present calculations and extracted data of $\underset{\sim}{\kappa}_{lat}(T)$ of c-Bi_2Te_3 from various sources.[19–28] Since Bi_2Te_3 is anisotropic, we focus on its tensor component $\kappa^{1,1}_{lat}$ along the basal plane of its hexagonal structure.[29]

Figure 1 shows the data on the lattice thermal conductivity $\kappa^{1,1}_{lat}$ along its basal plane[24–28] in the temperature region where the existing model calculation of this property has been carried out.[19–23] In order to understand the rather large scatter in the data, it is convenient to recall how this quantity is obtained. Until recently,[30–32] direct measurements of $\underset{\sim}{\kappa}_{lat}$ were hardly available, and one may also add that the new methods are not easy to implement. This is because they require very large magnetic fields $\boldsymbol{B}$ with respect to the charge carrier's mobility μ ($\mu B \gg 1$) even at intermediate temperatures (<150 K). These new methods will not be further discussed here as they have not yet been applied to Bi_2Te_3.

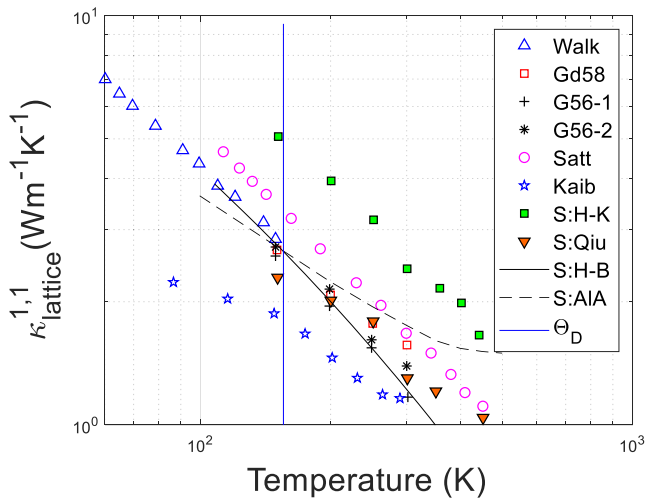

FIG. 1. Reported lattice contribution to the thermal conductivity of c-Bi_2Te_3 (symbols) along the basal plane of its hexagonal structure, as well as calculations of this quantity. The legend indicates principal authors' initials and the year of publication of the experimental data, obtained by digitizing figures in Refs. [24 and 25 (G56-1) to 28 (Kaib)]. Calculations (S:) correspond to Refs. [19 (H-K) to 23 (AlA)]. The vertical line indicates the Debye temperature Θ_D of c-Bi_2Te_3.

Hence, $\underset{\sim}{\kappa}_{lat}$ has mostly been extracted from a procedure that requires a thorough understanding of the electronic properties of the material, as well as accurate measurements of the total thermal conductivity tensor $\underset{\sim}{K}(T)$ as a function of temperature (T). One needs to obtain an accurate modelization of both the carriers' mobility $\underset{\sim}{\mu}_{e/h}$ and Seebeck coefficient $\underset{\sim}{S}_{e/h}$ for both majority and minority carriers in the temperature range of interest.[8] This is essential, as accurate values of both the electrical conductivity and the Lorenz coefficient $L(T)$ are required in order to calculate the electronic contribution to the thermal conductivity $\underset{\sim}{K}^{el}(T) = L(T)\underset{\sim}{\sigma}(T)T$ and thus obtain $\underset{\sim}{\kappa}_{lat} = \underset{\sim}{K} - \underset{\sim}{K}^{el}$. If, as is the case of the narrow gap material Bi_2Te_3, we are also required to determine $\underset{\sim}{\kappa}_{lat}$ in a temperature range where electron–hole pair excitations become significant, then the Lorenz coefficient $L(T)$ has to incorporate the thermodiffusion (or bipolar diffusion) component of thermal conductivity.[13] For example, a perusal of Ref. 28 reveals that the approximately exponential increase in the thermodiffusion term is absent in their computation of the Lorenz coefficient, and this is believed to be the cause of the (perhaps fictitious) increase in $\kappa^{1,1}_{lat}$ for the point at the highest temperature in their data (see Fig. 1). Meanwhile, earlier data were extracted at a time where the (non-parabolic) band structure of c-Bi_2Te_3 was poorly understood.

It should be noted, however, that this method of extraction has no major influence on the accuracy of $\underset{\sim}{\kappa}_{lat}$ at temperatures lower than ~25 K (about $\Theta_D/6$) as the following rough estimate indicates. At those temperatures, the metallic value (2.4×10^{-8} W Ω K^{-2}) is an upper bound of the Lorenz coefficient (in fact it is lower than ~2×10^{-8} W Ω K^{-2} according to Ref. 28), so for typical values of electrical conductivity ~5 MS m^{-1}, we obtain $K^{el}(T) < 1.2$ Wm^{-1}K^{-1} for T < 10 K. As we shall later show, this quantity is below ~4% of the value of the total thermal conductivity measured for c-Bi_2Te_3 at temperatures between 4 and 25 K.[33]

As for the model calculations of c-Bi_2Te_3 $\underset{\sim}{\kappa}_{lat}$, they range from the more recent Monte Carlo calculations of Ref. 23 using the relaxation time approximation to other diversified approaches of phonon transport starting from first principles or from *ab initio* molecular dynamic (AIMD) simulations. They usually involve the Phonon Boltzmann Transport Equation (PBTE) in combination with density functional theory (DFT) or density functional perturbation theory (DFPT), or AIMD. They are of interest not only for specific applications, as is the case with c-Bi_2Te_3, but mainly because phonon–phonon interactions, as well as interactions with other material degrees of freedom, are only partially understood. In the case of Bi_2Te_3, the combination of AIMD, which included explicitly the temperature dependence of the interatomic forces, with the iterative solutions of the PBTE gave the impressive results shown in Fig. 1, which appears to closely match two sets of experimental results.[22] Thus, these *ab initio* methods are apparently capable of great accuracy with no adjustable parameters, although one of their unstated assumptions appears to be the absence of scattering by crystal boundaries (CBs).[22] What is not clear yet is the degree with which that accuracy covers the whole temperature region, which should

include temperatures lower to the ones so far studied and shown in Fig. 1. In particular, AIMD simulations may require unaffordable computer resources at lower temperatures in order to thermally equilibrate the simulated system.

III. MODEL CALCULATION OF THE LATTICE THERMAL CONDUCTIVITY

It is unquestionable that the more advanced, computer intensive models mentioned above show significant progress when applied to crystalline material. What is surprising though is the lack of calculations, which compare with $\underset{\sim}{\kappa}_{lat}$ data for temperatures much lower than Θ_D. It is well known from basic solid state physics textbooks on thermal transport[34] that above Θ_D, the behavior of the lattice thermal conductivity of solids presents a smooth dependence $\sim T^{-x}$ with $x \sim 1$. Thus, calculations of $\underset{\sim}{\kappa}_{lat}$ in this temperature range do not furnish robust quantitative information about the mechanisms playing a significant role in its determination. This can be better understood through the simpler phenomenological models developed before 1963 in the studies of Klemens, Callaway, Holland, Carruthers, and others.[14–18] These approximate models, all based on the relaxation time approximation, convey a physical picture of the mechanisms involved. The applications of these models have clearly shown that the impact of these mechanisms is mostly revealed at temperatures below $\sim\Theta_D/3$ where the most significant changes in $\underset{\sim}{\kappa}_{lat}$ occur (in contrast to the smooth behavior above Θ_D).

It thus seems appropriate at this stage to apply such a model to the low temperature $\underset{\sim}{\kappa}_{lat}$ data of c-Bi_2Te_3, in order to obtain some guidance on the actual scattering mechanisms, which play a role in this compound at temperatures below 100 K. It gives the possibility to test the applicability of the approximate models at higher temperatures. In particular, it would allow us to determine the parameters that are intrinsic phonon properties of the crystal and are assumed to be independent of temperature, as will be examined in the discussion (Sec. IV C).

Given the anisotropy of c-Bi_2Te_3, we concentrate on a model for the component along the (hexagonal) a-axis of the basal plane $\kappa_{lat}^{1,1}$, which can be written as

$$\kappa_{lat}^{1,1} = \frac{f_a}{2f_a+1}\left(\frac{1}{V}\right)\sum_Q v_{Q\parallel}^2 \hbar\omega_Q \tau_Q \frac{\partial n_Q}{\partial T} \tag{1}$$

$[Q \equiv (\vec{q},p)]$, where p denotes mode polarization for a phonon of wave vector $\vec{q}$, $n_Q = \left\{\exp\left(\frac{\hbar\omega_Q}{k_BT}\right)-1\right\}^{-1}$, and $v_Q = v_Q(T) = \partial\omega_{\vec{q}}^p/\partial\vec{q}$ is the phonon group velocity, which is a temperature dependent quantity. The anisotropy factor $f_a = \frac{\kappa_{lat}^{1,1}}{\kappa_{lat}^{3,3}} = \frac{\kappa_{lat}^{2,2}}{\kappa_{lat}^{3,3}}$ remains unknown within this model and may even be temperature dependent. Notice that the value of the ratio $f_a/(2f_a+1)$ varies from 1/3 (from the isotropic case) to 1/2 for large anisotropy. Looking at *ab initio* calculations provided in the literature on a limited temperature range, one notices that the factor f_a is rather large. Estimates vary from ~1.6 to 3.2 according to the type of calculation.[19–22] For c-Bi_2Te_3, it was experimentally determined to be 2.1, with nearby values also for ternary alloys containing Sb and with Se.[35]

In Eq. (1), we will only keep the acoustical modes LA and TA, as it has been shown that the contribution of optical modes can be neglected for Bi_2Te_3,[19,23] and particularly so at low temperatures (more on this in Sec. IV A). Assuming degeneracy of TA modes and Debye dispersion for the phonon frequencies ω, it is easy to show that

$$\kappa_{lat}^{1,1} \approx \frac{f_a}{2f_a+1} 4\pi k_B \left(\frac{k_BT}{h}\right)^3 \times \left\{ \int_0^{\frac{\Theta_D}{T}} \frac{\left(v_g^{LA}/v_{ph}^{LA}\right)^2 x^4}{v_{ph}^{LA}\tau_{LA}^{-1}} \frac{e^x dx}{\left(e^x-1\right)^2} + \frac{2}{v_{ph}^{TA}} \int_0^{\frac{\Theta_D}{T}} \frac{x^4}{\tau_{TA}^{-1}} \frac{\left(v_g^{TA}/v_{ph}^{TA}\right)^2 e^x dx}{\left(e^x-1\right)^2} \right\}, \tag{2}$$

where v_g^p is the group velocity for polarity p, and the temperature dependence of the phase velocities $v_{ph}^p = v_{\Gamma-X}^p$ along $\Gamma - X$, for each mode, has been calculated from the elastic properties as measured in Ref. 36. For temperatures larger than a few Kelvins, we calculate the approximate expressions as follows:

$$\begin{aligned} v_{ph}^{LA} &\approx (2704 - 0.420\,76\cdot T[K])\ \mathrm{ms}^{-1}, \\ v_{ph}^{TA} &\approx (1754 - 0.3661\cdot T[K])\ \mathrm{ms}^{-1}, \end{aligned} \tag{3}$$

and we extend this approximation down to ~2 K. Notice that in order to be entirely consistent with the Debye approximation of the phonon dispersion relations, we will have to further assume that $\left(v_g^p/v_{ph}^p\right) \approx 1$ for both acoustic modes. In Sec. IV A, we will see that this approximation may be marginally reasonable for the low temperatures considered. In Sec. IV C, we will also discuss the absence of another term in Eq. (2), which appears in the Callaway version of the model,[15,16] and the fact that we have ignored it will be shown to be self-consistent with the values obtained for the phenomenological parameters.

In accordance with Matthiessen's rule, the scattering rate for longitudinal acoustic (LA) phonons can be written as

$$\tau_{LA}^{-1} = \underbrace{\left(v_{av}(T)/L_g\right)}_{c-\text{boundaries}} + \underbrace{dxT}_{Disloc} + \underbrace{\beta_L x^2 T^5}_{\text{N,L}} + \underbrace{\varphi_U x^2 T^3 \exp\left(-\Theta_D/nT\right)}_{\text{U}} + \underbrace{\alpha x^4 T^4}_{\text{I/D}}, \tag{4}$$

where $x \equiv \hbar\omega/k_BT = h\nu/k_BT$, and the temperature dependent average velocity is defined by the following expression:

$$\frac{3}{v_{av}(T)} = \left(\frac{1}{v_{ph}^{LA}(T)} + \frac{2}{v_{ph}^{TA}(T)}\right). \tag{5}$$

For the transverse acoustical (TA) modes,

$$\tau_{TA}^{-1} = \left(v_{av}(T)/L_g\right) + dxT + \underbrace{\beta_T x T^5}_{\text{N,T}} + \varphi_U x^2 T^3 \exp\left(-\Theta_D/nT\right) + \alpha x^4 T^4. \tag{6}$$

In both Eqs. (4) and (6), the number n, which evaluates the activation energy of Umklapp (U) processes and is sometimes taken as $n = 3$, has been left as an adjustable parameter, as is the average grain size L_g. The other phenomenological parameters involved in

TABLE I. List and definition of the parameters included in the scattering rates of Eqs. (4) and (6) to calculate the lattice thermal conductivity in our Debye-type model. The identifying symbols and the physical units, which will be used to present numerical values, are also included.

Parameter definition	Symbols and units $x \equiv \hbar\omega/k_BT = h\nu/k_BT$
N-process, LA mode	$B_{N,L} = (\hbar/k_B)^2\beta_{N,L}$ (10^{-22} s K^{-3}); $\tau_{NL}^{-1} = \beta_{N,L}x^2T^5 = B_{N,L}\omega^2T^3$
N-process, TA mode	$B_{N,T} = (\hbar/k_B)\beta_{N,T}$ (10^{-12} K^{-4}); $\tau_{NT}^{-1} = \beta_{N,T}xT^5 = B_{N,T}\omega T^4$
Umklapp process	$C_U = (\hbar/k_B)^2\varphi_U$ (10^{-18} s K^{-1}); $\tau_U^{-1} = \varphi_U x^2T^3e^{-\Theta_D/nT} = C_U\omega^2Te^{-\Theta_D/nT}$
Impurities and defects	$B_{I/D} = \alpha(\hbar/k_B)^4$ (10^{-41} s^3); $\tau_{I/D}^{-1} = \alpha x^4T^4 = B_{I/D}\omega^4$
Dislocations	$D = d(\hbar/k_B)$ (dimensionless); $\tau_\omega^{-1} = dxT = D\omega$
Crystal boundaries	$\tau_{CB}^{-1} = v_{av}/L_g$; v_{av}: average speed in bulk, L_g: average grain size
Average sound velocity	v_{av}(T) (10^3 m/s): calculated according to Eq. (5)

these equations are identified in Table I. The expressions adopted for the frequency dependence of most of these parameters are the usual ones, developed in the work of Refs. 14–18. The first, second, and third rows in Table I correspond to phonon–phonon interactions for Normal (N), Longitudinal (L, LA), and Transverse (T, TA) acoustical modes and U processes. The term corresponding to U processes, is usually written as shown in Eq. (4), instead of the expression proposed by Holland.[17] The fourth row (I/D) involves impurities and/or defects, excluding dislocations (core and strain field). The role of dislocation strain field we consider is shown in the fifth row, with a rate that is independent of temperature and proportional to frequency.[14] In the sixth (and seventh) row, the rate that corresponds to limitations imposed by crystal boundaries (CBs) is independent of phonon frequency, as originally derived.

A re-examination of the Callaway model comparing its results to an accurate iterative solution of the PBTE has shown that U-process rates may scale as the cube power of the frequency for some semiconductors.[37] However, after comparing both versions to various datasets, we have adopted the expression in Eqs. (4) and (6) ($\propto \omega^2Te^{-\Theta_D/nT}$), yielding better fits. In contrast, the frequency dependence of the N-process for the transverse mode, which has been adopted [in Eq. (6) and Table I], corresponds to that suggested by the same calculations of Ref. 37. The often used expression for the LA mode ($\propto \omega^2T^3$) has been kept, as it was also corroborated by the calculations in Ref. 37.

Some of the parameters shown in Table I have in the past been modeled in terms of basic physical constants and related properties of the solid, such as structure, sound velocity, Grüneisen parameter, and average mass. Expressions were obtained under simplifying assumptions, which may not apply to a complex material such as Bi_2Te_3 and will not be adopted here. In the present application of the model determined by Eqs. (2)–(6), we select a set of free parameters representing the scattering processes, such as (β_L, β_T, φ_U, α, d, n, L_g), in Table I. Then, a systematic search algorithm was used to minimize the root mean square error (RMSE) when fitting the $\kappa_{lat}^{1,1}$ data, including the low temperature region of Ref. 33. This minimization allowed the determination of optimized numerical values for ($B_{N,L}$, $B_{N,T}$, C_U, $B_{I/D}$, D, n, L_g), the parameters of interest. The Debye temperature Θ_D in Eq. (2) was fixed at the empirically determined value $\Theta_D \approx 155.5$ K.[1] More details on the calculations will be given when we present the results in Sec. IV.

The term proportional to the phonon angular frequency of the form $\tau_\omega^{-1} = D\omega = dxT$, where the dimensionless parameter $D = (\hbar/k_B)d$ is often attributed to scattering of phonons by strain field of dislocations, has been incorporated in the explicit description of our model. Such a term appears important to assure fitting procedures that minimize the RMSE. However, it usually delivered values of D such that its contribution to the lattice thermal conductivity can be neglected below 150 K, as is also the case of $B_{N,L}$. The almost negligible impact of these scattering mechanisms will be further discussed in Sec. IV C.

IV. RESULTS AND DISCUSSION

Before we present the results of the model, we need to discuss the only existing thermal conductivity data that could be found in the literature for c-Bi_2Te_3 reaching temperatures as low as ~2 K.[33] This work of MacDonald *et al.* was mainly concerned with TE refrigeration for the attainment of very low temperatures. Their presentation of the data is succinct (no uncertainties), and there is no specific attempt to extract the lattice thermal conductivity. As we have already discussed in Sec. II, for temperatures below ~25 K, the thermal conductivity of c-Bi_2Te_3 is practically undistinguishable from the total thermal conductivity, so we will consider their measurements directly, with no attempt to correct it for the (much smaller) electronic contribution. A comparison with the data of Ref. 27 in the temperature range where they overlap justifies this approximation (compare the two datasets in the range ~8–20 K in Fig. 2).

More problematic is the absence of presentation of the crystal quality of the samples used to measure this property.[33] Since the samples are most likely the result of directional solidification, the grains are expected to be fairly large in comparison with polycrystalline materials but no larger than hundreds of micrometers for this difficult to grow compound. By including the average grain size parameter L_g in the fit optimization procedure, we can approximately account for our ignorance on crystal structure. We have noticed, however, that if we fix values of L_g and n and then run optimizations to fit the data with the reduced set of parameters (β_L, β_T, φ_U, α, d), we can also obtain fits of comparable quality, which turn out to be slightly better at temperatures below 3 K, when a fixed value of $L_g = 125$ μm is used. As a consequence, the results to be shown in Sec. IV A will show parameters associated with these two fitting approaches.

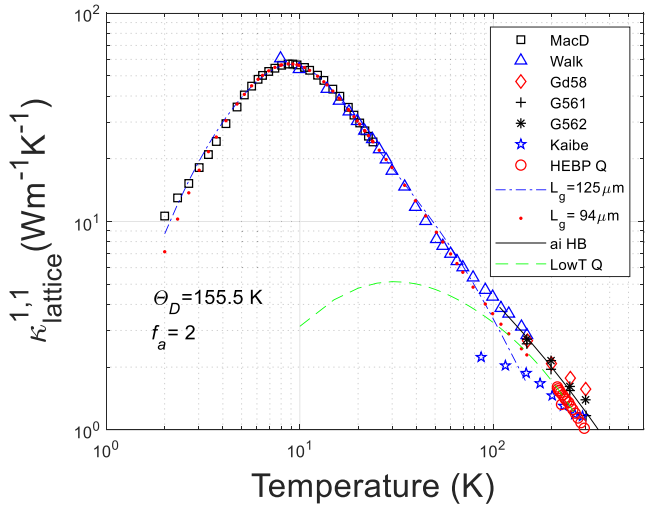

FIG. 2. c-Bi_2Te_3 lattice thermal conductivity $\kappa_{lat}^{1,1}$ in the basal plane as a function of temperature. Data from Ref. 33 (squares), Ref. 27 (triangles), Ref. 25 (diamonds), Ref. 24 (crosses and stars), and Ref. 28 (pentagrams). The datasets are compared to the simulated values calculated by the Debye-like model of Eq. (2), with (i) the optimized set of parameters shown in Table II for f_a = 2 (dots) and (ii) those in parentheses in the same column, with L_g = 125 μm (dotted-dashed curve). The *ab initio* molecular dynamics calculation of Ref. 22 above 100 K (solid line) is also shown, as well as data of a hot extruded quaternary alloy (circles, adapted from Ref. 8) and its simulation (dashed curve, Ref. 13).

As for the lack of knowledge of the actual, possibly temperature dependent, anisotropy parameter f_a, we have adopted a value independent of temperature. Simulations were carried out independently varying this quantity between its expected limits, which were already discussed in Sec. III. We will discuss the impact of this parameter after the presentation of the results.

A. Application of the dispersionless Debye model

Figure 2 shows the low temperature data of MacDonal *et al.*[33] combined with that of Refs. 24–28 as well as the best fit that can be obtained with the model of Sec. III, taking the anisotropy factor independent of temperature. Note that the whole dataset covering up to 300 K is shown in Fig. 2, while the two best fits (dotted and dotted-dashed curves) were obtained only for the data below 149 K taken from Refs. 33 and 27. This figure illustrates the quality and limitations of the fit that can be obtained with the Debye-type model we have proposed in Eq. (2), where $\left(v_g^p/v_{ph}^p\right) = 1$, with the anisotropy factor f_a = 2 or 1.9 (both give the same RMSE). Fitting curves with larger or smaller anisotropy factors are not as good, with an RMSE rapidly increasing as we depart from the two optimum values.

The following procedures were used to determine the optimized parameter values, which are shown in Table II (second and third columns). We numerically defined a function $\psi_{\kappa_L^{1,1}}(T, \boldsymbol{x}_0)$, which calculates the value of the lattice contribution to the thermal conductivity following the expression of Eq. (2), where the "free" parameters appearing in Eqs. (4) and (6) are represented by the array $\boldsymbol{x}_0 = (\beta_L, \beta_T, \varphi_U, \alpha, d, n, L_g)$, as the Debye temperature Θ_D = 155.5 K has been determined for c-Bi_2Te_3.[1] From the two optimized sets

TABLE II. Rate coefficients determined by the constrained optimization of the fit to lattice thermal conductivity data of c-Bi_2Te_3 along the basal plane in the temperature range from ~2 to 149 K, using $\Theta_D \approx$ 155.5 K(columns 2 and 3). The fourth column (MC) corresponds to the work on c-Bi_2Te_3 of Ref. 23 determined for 100 K < T < 500 K. The last column results from a simulation of a poly-c quaternary alloy in the range from 200 to 430 K. The values in parentheses in column 3 correspond to minimizations, where L_g = 125 μm has been separately adjusted providing a slightly better visual fit to data for temperatures below 3 K.

Property (units)	f_a = 1.9	f_a = 2	MC[a]	N33 (Q)[b]
$B_{N,L}$ (10^{-22} s K^{-3})	<5.2 × 10^{-4}[c]	<5.2 × 10^{-4}[c]	3.604	1.45
$B_{N,T}$ (10^{-12} K^{-4})	1545	1566 (272.8)	968.1	2.90
C_U (10^{-18} s K^{-1})	6.44	6.50 (12.95)	1.125	14.0
$B_{I/D}$ (10^{-41} s^3)	0.156	0.157 (0.233)	0.639	3.06
D	9291.6	9286.4 (~10^{-16})	N/A	(~10^{-8})
L_g (μm)	95.6	94.5 (125)	N/A	1200

[a] Values taken from Ref. 23, case 2.
[b] Adapted from Ref. 13, using n = 3.
[c] Repeated numerical optimizations give the same RMSE with slightly different $B_{N,L}$ values.

$\boldsymbol{x}_0^{Op} = (\beta_L, \beta_T, \varphi_U, \alpha, d, n, L_g)^{Op}$ corresponding to f_a = 1.9 (second column) and f_a = 2 (third column), we obtained the parameters shown in Table II, following their definition shown in Table I. These optimization procedures are constrained by a lower bound $\boldsymbol{x}_0 = \boldsymbol{0}$ (all parameters positive).

In a separate procedure, L_g and n were left out of the free parameter set, now defined as $\boldsymbol{y}_0 = (\beta_L, \beta_T, \varphi_U, \alpha, d)$. In this second approach, the value of n was fixed to that produced by the previous optimization (n = 4.333) and L_g was given various fixed values while numerically proceeding to optimize $\boldsymbol{y}_0$ through fitting $\psi_{\kappa_L^{1,1}}(T, \boldsymbol{y}_0)$ to the data. The values in parentheses of the third column are obtained from $\boldsymbol{y}_0^{Op} = (\beta_L, \beta_T, \varphi_U, \alpha, d)^{Op}$ with L_g = 125 μm. While the value of n = 4.333 has been determined with no ambiguity, the effect of changing the crystal-boundary size L_g, and hence τ_{CB}^{-1}, is more difficult to assess. The root mean square error or RMSE associated with the fitting function is strictly minimized for L_g = (94.5 ± 1) μm. Lower values of L_g rapidly increase the RMSE, and higher values do so but much less rapidly. However, as Fig. 2 clearly illustrates, the fitting at L_g = 125 μm is slightly better at temperatures lower than 3 K. Values larger than 125 μm only increase the RMSE with no visible gain in low temperature fitting. Since we do not have the structural data, we cannot be certain as to which of the two sets of values is a better choice, so both have been presented in the figure and in Table II for f_a = 2. We note as a reminder that the lower temperature region is the one where the expressions of the phonon scattering rates have been developed.[14,15] It is worth pointing out that despite the differences in the values of the parameters shown in column 3 of Table II, the spectral distributions $\kappa_{lat}^{1,1}(\nu, T)$ for both optimized sets shown in column 3 do not differ much. We show $\kappa_{lat}^{1,1}(\nu, T)$ in Fig. 3, only for the values of the optimized parameters $\boldsymbol{x}_0^{Op} = (\beta_L, \beta_T, \varphi_U, \alpha, d, n, L_g)^{Op}$; the corresponding figure for the parameters in parentheses in column 3 of Table II would be practically indistinguishable. For example, the maximum of 0.132 nJ/mK for $\kappa_{lat}^{1,1}(\nu, T)$ shown in Fig. 3 occurs at ν_m = 0.292 THz, T_m = 6 K, while the corresponding maximum with the parameters

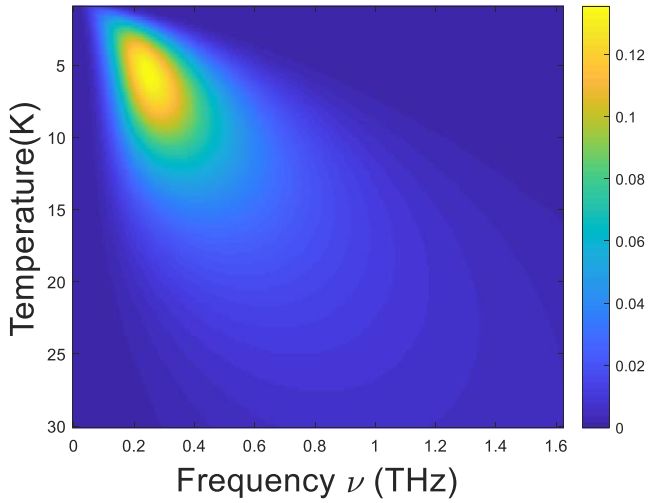

FIG. 3. Spectral distribution of c-Bi_2Te_3 lattice thermal conductivity $\kappa_{lat}^{1,1}(\nu, T)$ in units of nJ/m K as a function of temperature and frequency, calculated with the optimized parameters given in column 3 of Table II. The corresponding distribution calculated with the values in parentheses of column 3, Table II, would be visually indistinguishable from this figure.

shown in parentheses in column 3 of Table II is 0.136 nJ/mK at ν_m = 0.253 THz, T_m = 5.8 K. Further discussion of these choices is left to Sec. IV C.

We have also calculated the spectral contribution of separate scattering mechanisms (not shown). The important observation is that in the region of interest shown in Fig. 3, the intensity of the spectral contribution, which only includes the U processes rate $[\kappa_U^{1,1}(\nu, T) \propto \tau_U(\nu, T)]$, is larger by a factor ~10^3–10^{12} compared to the intensities shown in the figure. This intensity is rapidly reduced when the I/D and subsequent rates are added to $\kappa_U^{1,1}(\nu, T)$.

Table II also shows, for comparison purposes, the results on c-Bi_2Te_3, as determined in the work of Ref. 23 obtained from Monte Carlo solutions of the PBTE in the temperature range from 100 to 500 K (see column 4).

In previous work, the lattice thermal conductivity of hot extruded bulk polycrystalline (HEBP) $(Bi_{1-x}Sb_x)_2(Te_{1-y}Se_y)_3$ ternary and quaternary alloys was extracted[8] and simulated[13] with a model similar to the one presented here. Since these are highly textured materials along the extrusion axis (ex), their measured thermal conductivity is anisotropic with the ratio $K_{\parallel ex}/K_{\perp ex} \approx 1.5$ with some variations depending on the experimental conditions. In the last (fifth) column of Table II, we show the values of the parameters obtained from the lattice thermal conductivity along the extrusion axis for a HEBP quaternary alloy sample N0303 ($x = y = 0.03$), which is representative of alloys whose composition is close to the base compound. This optimization fits data covering the range 200 K < T < 430 K,[13] and the parameters obtained were then used to extend the simulation to lower temperatures as shown by the dashed (labeled Low T Q) curve in Fig. 2. The model simulation is Debye-like, where the prefactor due to anisotropy is approximated as $\frac{f_a}{f_a+2} \approx \frac{1}{3}$ in place of $\frac{f_a}{2f_a+1}$ [see Eq. (2)], since due to texture introduced by extrusion, the basal planes of the HEBP grains tend to align along the extrusion direction ($\parallel ex$).

B. Mean free path

The spectral decomposition $\underset{\sim}{\kappa}_{lat}(\omega)$ is often carried out in the literature at a fixed temperature. $\underset{\sim}{\kappa}_{lat}(\omega)$ depends strongly on the proposed model and in particular, when a simplified model for the PDOS, like the Debye approximation, is used, the result could be of limited value, particularly at larger temperatures. The same can be said of the spectral dependence of the phonon mean free path, which is calculated for each polarization "p" as $\Lambda_{ph}^{T,p}(\omega) = v_g^p(\omega, T)/\tau_p^{-1}(\omega, T)$; since in a Debye-like model $v_g^p(\omega, T) = v_{ph}^p(T)$, substantial information could be lost in this calculation for temperatures high enough to excite higher frequency modes. One could introduce a model for $v_g^p(\omega, T)$, but doing so would not provide a self-consistent calculation. The calculation of $\kappa_{lat}^{1,1}(\nu, T)$ that we have provided in Fig. 3 shows that in the particular case of c-Bi_2Te_3, this approximation may be marginally satisfied for temperatures below ~150 K. Note that most of the contribution occurs below $\nu \leq 0.4$ THz, where an approximately linear dispersion relation may be a fair approximation for c-Bi_2Te_3.

There is, however, another quantity of interest, which is the phonon average mean free path (mfp) $\langle \Lambda_{ph}(T) \rangle$, a function of temperature, calculated (in the basal plane, b) as

$$\langle \Lambda_{ph} \rangle_b = \frac{3(\kappa_{\rm lat}(T))_b}{c_V(T) v_{av}(T)}, \tag{7}$$

where c_V is the specific heat at constant volume, and the average velocity is given by Eq. (5).

In order to compute the average mfp of Eq. (7), we need to calculate the heat capacity at constant volume C_V, in the Debye approximation. This quantity is slightly smaller but comparable to C_P (at constant pressure) for which data are available for Bi_2Te_3. The calculation results and data are presented in Fig. 4. It is easier to measure the heat capacity at constant pressure C_P, while the difference between C_V and C_P is very small for solids and is given by

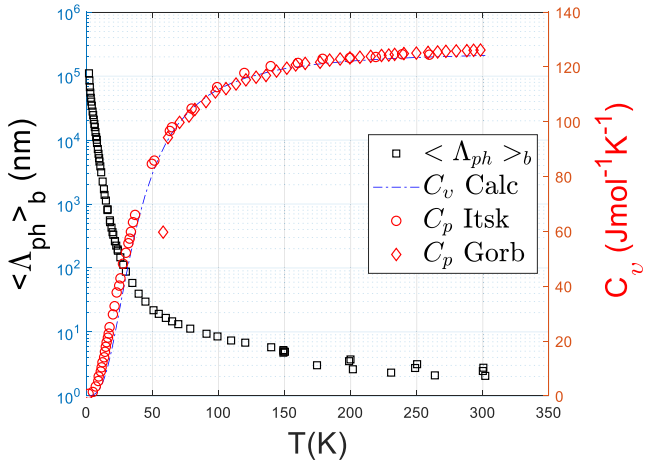

FIG. 4. Calculation of the phonon average mean free path $\langle \Lambda_{ph}(T) \rangle_b$ (empty black squares, scale on the left), as a function of temperature as determined from Eq. (7). The calculated molar heat capacity at constant volume is shown by the dotted-dashed (blue) line scale on the right, compared with data on C_p from Ref. 38 (circles) and Ref. 39 (diamonds).

$\Delta C = C_P - C_V = 9\eta_T^2 T\Omega/K_{iso}$, where η is the thermal expansion coefficient, K_{iso} is the isothermal compressibility, and Ω is the molar volume. The relative difference for Bi_2Te_3 can be estimated at ambient temperature and remains smaller than $\frac{\Delta C}{C} \approx \frac{9\times10^{-2}}{120} \approx 8\times10^{-4} \ll 1$.

The range of values of the average mfp for this compound below Θ_D extends for five orders of magnitude.

C. Discussion and implications of the simple model

We recall that the optimization procedure followed to obtain $\kappa_{lat}^{1,1}$ as a function of temperature, explained in Sec. IV A, was essentially geared to determine the set of parameters shown in Table II, obtained by optimizing the fit of $\psi_{\kappa_L^{1,1}}(T, \boldsymbol{x}_0)$ to the data, considering the seven free parameters $\boldsymbol{x}_0 = (\beta_L, \beta_T, \varphi_U, \alpha, d, n, L_g)$. In fact, given our lack of knowledge of the crystalline structure of the sample from which we obtained the low temperature data,[33] the crystal-boundary size L_g, and hence τ_{CB}^{-1}, also needed to be determined. Here, we review and discuss our implementation of the optimization process, which was carried out in essentially two ways. First, we used all seven parameters as free variables to be optimized by minimizing the RMSE of the fit to the data for temperatures below 149 K, which allowed the determination of n = 4.333, and the six parameters shown in Table II, columns 2 and 3 for only two values of the anisotropy parameter giving the lowest (and the same) value of the RMSE. The second approach adopted f_a = 2 and the optimized value of n (=4.333), and thus, the activation enthalpy for the rate of U scattering processes is $\Delta h^U = k_B\Theta_D/n \approx 3.1$ meV. By fixing a value of L_g, we then reduced the number of free parameters to 5 $\boldsymbol{y}_0 = (\beta_L, \beta_T, \varphi_U, \alpha, d)$. In this case, it was found that when L_g = 125 μm, the fit for f_a = 2 looked better for temperatures below 3 K and was practically undistinguishable to the previously found for temperatures below 100 K (see Fig. 2). The conclusions summarized in Table II, column 3, were corroborated by repeating the process of restricting the number of free parameters. For example, we tried varying the value of n by fixing L_g = 125 μm such that by fixing a value of n, we optimized $\boldsymbol{y}_0 = (\beta_L, \beta_T, \varphi_U, \alpha, d)$. In this case, for f_a = 2, a range of values 4.29 < n < 4.34 gave fitting curves with the RMSE close to the optimized one at 4.333. We also noticed that the parameter d, related to dislocation strain, could not be ignored to obtain convergence in the fitting procedure, even though its inclusion usually gave negligible values for D. Note that the two values of D quoted in column 3 of Table II, differing by various orders of magnitude, hardly impact the quality of the fits (both shown in Fig. 2). The spectral distribution of Fig. 3, as was remarked in Sec. IV A, also remained practically unchanged for both sets of values. The physical reason why the dislocation strain field has almost zero impact on the results at low temperatures may be understood precisely by the spectral distribution of Fig. 3. For the low temperature data considered, Fig. 3 gives us two important hints: (i) the use of a Debye approximation may be approximately correct as phonons whose frequency is larger than about 0.4 THz do not appear to participate, so a quadratic PDOS is an acceptable approximation, and, more important, (ii) the phonon energy remains low. According to a recent molecular dynamic study of phonon scattering by the strain field of a dislocation in PbTe, only medium and high energy phonons are expected to be affected[40] by this strain field. On the basis of this result, one may speculate that this is also the case for the strain field of a dislocation in Bi_2Te_3.

Next, we discuss one weakness of the model, which is the unknown value of the (thermal) anisotropy parameter f_a. Reports of various calculations in the literature (see Fig. 5 in Ref. 23) indicate that the lattice thermal conductivity anisotropy may vary with temperature and have temperature dependent values. The only experimental value of f_a for c-Bi_2Te_3 is 2.1 at ambient temperature,[35] with no measurement of temperature variation. We first note that the quality of the fit for temperatures below 149 K is not affected by the choice 1.9 < f_a < 2 and although f_a values outside this range do not provide as good matches to experiment for the whole 2 < T < 149 K range, as indicated by an increase in the RMSE, they are visually acceptable for f_a slightly larger than 2. In Table II, we have not included simulations with the isotropic value (f_a = 1), which gives quantitative values of the four parameters very different to the ones shown. In particular, the value $C_U \approx (14.4 \pm 0.5)\times10^{-18}$ s · K^{-1} (obtained for f_a = 1) for the Umklapp process came close to values obtained for ternary and quaternary alloys of HEBP samples (the last column of Table II).

The $B_{I/D}$ values, which are close for $f_a \approx 2$ in the crystal (columns 2 and 3), are consistently lower than those obtained for extruded polycrystalline samples, as expected. For the normal process, the parameter for the longitudinal mode $B_{N,L}$ is not dependent on the choice of optimization but the negligible small values obtained remain unexplained. It is worth remarking that simulations were carried out to verify if the negligible value for $B_{N,L}$ does not result from changing the expression of $\tau_{N,T}^{-1}$ as a function of frequency (here proportional to $\tau_{N,T}^{-1} \propto \omega T^4$, see Table I). Had we chosen $\tau_{N,T}^{-1} \propto \omega^2 T^3$, as the expression for the longitudinal mode $\tau_{N,L}^{-1}$, the quality of the fit is somewhat diminished, yet the value of the parameter $B_{N,L}$ still remains negligibly small. For the transverse acoustical mode, the $B_{N,T}$ value depends on the choice of fitting procedure (see column 3, Table II); However, the discrepancy in values does not appear to significantly change the quality of the fitting (Fig. 2) nor the spectral distribution of Fig. 3. It appears that the role of N processes, usually associated with affecting only the non-equilibrium phonon distribution, contributes little to lattice heat transport in c-Bi_2Te_3.

The above observation helps us understand why Callaway's term applying only to longitudinal acoustical modes, and neglected in Eq. (2), which is

$$t_{negl} = \frac{\left[\int_0^{\frac{\Theta_D}{T}} \frac{x^4\tau_{N,L}^{-1}}{\tau_{LA}^{-1}} \frac{e^x dx}{(e^x-1)^2}\right]^2}{\int_0^{\frac{\Theta_D}{T}} x^4\tau_{N,L}^{-1}\left(1-\frac{\tau_{N,L}^{-1}}{\tau_{LA}^{-1}}\right)\frac{e^x dx}{(e^x-1)^2}}, \tag{8}$$

can be safely ignored in a self-consistent approach. We just need to compare it with the term that was included to conclude that

$$\frac{t_{negl}}{t_{incl}} \approx \frac{\left[\int_0^{\frac{\Theta_D}{T}} \frac{x^4\tau_{N,L}^{-1}}{\tau_{LA}^{-1}} \frac{e^x dx}{(e^x-1)^2}\right]}{\int_0^{\frac{\Theta_D}{T}} \frac{x^4}{\tau_{LA}^{-1}} \frac{e^x dx}{(e^x-1)^2}} \ll 1.$$

We have also compared in Table II (fourth column, titled **MC**) the values obtained in Ref. 23 using Monte Carlo phonon transport modeling in a temperature range above 100 K, where these values clearly differ from the ones that we have obtained at lower

temperatures. This may be a consequence of trying to extend the validity of the Klemens–Callaway–Debye model to a temperature range ($>\Theta_D$) where it was not conceived to apply. If the phenomenological model would still apply at larger temperatures, then it would be expected that $B_{N,L}$, $B_{N,T}$, and $C_{U,L}$ remain intrinsic material properties of c-Bi_2Te_3, which are independent of temperature. However, if we fix the values of $B_{N,L}$, $B_{N,T}$, and $C_{U,L}$ to those in parentheses of the third column of Table II and run simulations to fit the high temperature data (where we excluded the measurements of Ref. 28), our simulations are unable to provide satisfactory fittings up to 300 K.

We have also attempted simulations of the HEBP quaternary data keeping as values of $B_{N,L}$, $B_{N,T}$, and $C_{U,L}$ those (within parentheses) of the third column of Table II. Our simulations for the temperature range 200 K–430 K, where we have data, are unable to provide a reasonable fit. In this case, however, it may be argued that a quaternary, even one close to the binary where $x = y = 0.03$, is a different material than c-Bi_2Te_3, and particular so, given that it is polycrystalline (average grain size close to 1–2 μm). So, even if both the HEBP alloys and the base compound have a lattice thermal conductivity, which appear to be limited by the same set of scattering mechanisms than c-Bi_2Te_3, these parameters have different values, as if they were extracted from different materials. It is perhaps another indicator that extending the phenomenological models based on the Debye–Klemens–Callaway approach to temperatures higher than Θ_D does not provide a correct understanding of thermal transport.

Although Fig. 2 indicates that a good quality fit can be obtained to the lattice thermal conductivity of c-Bi_2Te_3 at temperatures below 149 K, we believe that Table II only highlights the dismal state of our knowledge of the thermal properties of this material, which has been under investigation since the late 1950s. The quality of the fit at low temperatures simply corroborates that the phenomenological approach that had been developed by Klemens, Callaway, and Holland[14–17] consistently applies *only* in the low temperature range. Moreover, it may be questionable to forcefully implement it in a temperature range above ~100 K, as appears to be the case in the most recent literature[41–43] on TE material development.

V. CONCLUSION

The presently known data and modelization of the lattice thermal conductivity $\kappa_{lat}^{1,1}(T)$ of crystalline Bi_2Te_3, involving temperatures above 100 K, have been briefly reviewed, together with models developed to understand its mechanisms of thermal transport. A simplified phenomenological model was developed based on the relaxation time approximation, with a Debye approximation to the phonon density of states, following the studies originally developed before the mid-1960s to model the low temperature behavior of $\underset{\sim}{\kappa}_{lat}(T)$. This model provides a fit to the known data in the range 2 K up to 150 K, which includes the low temperature range below 100 K, previously ignored in the existing literature. The phenomenological parameters associated with phonon–phonon scattering that were obtained do not entirely agree with those previously obtained by others when modeling thermal transport in crystalline Bi_2Te_3 above 100 K. The extension of the present model to higher temperatures, keeping the values of the intrinsic material parameters associated with phonon–phonon scattering, cannot provide a satisfactory fit to the data for crystalline Bi_2Te_3 up to 300 K, nor to other Bi_2Te_3 based materials in the 200–430 K range. We considered in particular typical polycrystalline alloys close to Bi_2Te_3 synthesized by hot extrusion, of relevance for industrial applications. When fixing the phonon scattering parameters to those of the low temperature crystal, one cannot adequately describe the higher temperature thermal transport. This is most likely due to the fact that the model comprises approximations, which only apply to temperatures below the Debye temperature. This work signals that attempting to understand and examine thermal transport based on the approximations involved in the pioneering work of Klemens–Callaway–Holland and Carruthers is not justified except below the Debye temperature. The temperature ranges of interest for most materials currently considered for thermoelectric applications remain outside this "allowed" range of present phenomenological models, despite its frequent use in the literature.

ACKNOWLEDGMENTS

We acknowledge the financial assistance of the Natural Sciences and Engineering Research Council of Canada (NSERC) for support through the Discovery Grants program, Grant No. RGPIN-2016-06417. We acknowledge as well the support of the Fonds de recherche du Québec-Nature et technologies (FRQ-NT).

AUTHOR DECLARATIONS

Conflict of Interest

The author declares that he has no conflicts to disclose.

Author Contributions

Remo A. Masut: Conceptualization (lead); Data curation (lead); Formal analysis (lead); Funding acquisition (lead); Investigation (lead); Methodology (lead); Resources (lead); Software (lead); Validation (lead); Visualization (lead); Writing – original draft (lead); Writing – review & editing (lead).

DATA AVAILABILITY

The data presented in the article was gathered from various references, which were duly cited.

NOMENCLATURE

k_B	Boltzmann constant (1.38×10^{-23} kg m^2 s^{-2})
$\hbar$	reduced Planck constant (1.055×10^{-34} J s)
$\underset{\sim}{K}$	thermal conductivity tensor (W m^{-1} K^{-1})
$\underset{\sim}{K}^{el}$	electronic contribution to thermal conductivity (W m^{-1} K^{-1})
$\underset{\sim}{\kappa}_{lat}$	lattice thermal conductivity tensor (W m^{-1} K^{-1})
L	Lorenz coefficient (W Ω K^{-2})
$\underset{\sim}{\mu}_{e/h}$	carrier (e/h) mobility tensor (m^2 V^{-1} s^{-1})
Θ_D	Debye temperature (K)
σ	electrical conductivity (Ω^{-1} m^{-1} = S m^{-1})

S	Seebeck coefficient (V K^{-1})
T	temperature (K)
τ_λ^{-1}	total scattering rate of phonons of mode λ
ν	phonon frequency (Hz)
ω	angular frequency ($2\pi\nu$) (rad Hz)
AIMD	*ab initio* molecular dynamics simulations
CBs	crystal boundaries
DFPT	density functional perturbation theory
DFT	density functional theory
HEBP	hot extruded bulk polycrystalline
I/D	impurities and/or defects
LA	longitudinal acoustical phonon mode
MC	Monte Carlo
PBTE	phonon Boltzmann transport equation
PDOS	phonon density of states
TA	transverse acoustical phonon mode
TE	thermoelectric

REFERENCES

[1] G. S. Nolas, J. Sharp, and H. J. Goldsmid, *Thermoelectrics: Basic Principles and New Materials Developments* (Springer, Berlin, 2001), see Chap. 5 and references therein covering before the year 2000.

[2] Y. L. Chen, J. G. Analytis, J.-H. Chu, Z. K. Liu, S.-K. Mo, X. L. Qi, H. J. Zhang, D. H. Lu, X. Dai, Z. Fang *et al.*, "Experimental realization of a three-dimensional topological insulator, Bi_2Te_3," Science **325**, 178–181 (2009).

[3] J. M. Raju and K. J. Thomas, "Topological insulator phases in polycrystalline Bi_2Te_3 thin films," AIP Adv. **13**, 025045 (2023).

[4] J. K. Lee, S. Park, B. Ryu, H. S. Lee, J. Park, and S. Park, "Effect of defect interactions with interstitial Ag in the lattice of $Bi_xSb_{2-x}Te_3$ alloys and their thermoelectric properties," Appl. Phys. Lett. **118**, 052102 (2021).

[5] H.-L. Zhuang, J. Pei, B. Cai, J. Dong, H. Hu, F.-H. Sun, Y. Pan, G. J. Snyder, and J.-F. Li, "Thermoelectric performance enhancement in BiSbTe alloy by microstructure modulation via cyclic spark plasma sintering with liquid phase," Adv. Funct. Mater. **31**, 2009681 (2021).

[6] A. Jena, S.-C. Lee, and S. Bhattacharjee, "Tuning the lattice thermal conductivity in bismuth telluride via Cr alloying," Phys. Rev. Appl. **15**, 064023 (2021).

[7] F. Guo, Y. Sun, H. Qin, Y. Zhu, Z. Ge, Z. Liu, W. Cai, and J. Sui, "BiSbTe alloy with high thermoelectric and mechanical performance for power generation," Scr. Mater. **218**, 114801 (2022).

[8] R. A. Masut, C. André, and D. Vasilevskiy, "Hot extruded bulk polycrystalline $(Bi_{1-x}Sb_x)_2(Te_{1-y}Se_y)_3$ alloys: Electron transport and lattice thermal conductivity," J. Electron. Mater. **52**, 707–717 (2023).

[9] J. Lee, H. Sul, W. Lee, K. R. Pyun, I. Ha, D. Kim, H. Park, H. Eom, Y. Yoon, J. Jung, D. Lee, and S. H. Ko, "Stretchable skin-like cooling/heating device for reconstruction of artificial thermal sensation in virtual reality," Adv. Funct. Mater. **30**, 1909171 (2020).

[10] W. Zhu, P. Wei, J. Zhang, L. Li, W. Zhu, X. Nie, X. Sang, Q. Zhang, and W. Zhao, "Fabrication and excellent performances of bismuth telluride-based thermoelectric devices," ACS Appl. Mater. Interfaces **14**, 12276–12283 (2022).

[11] Y. Wang, L. Yang, Y. Zheng, D. Wang, and Y. Deng, "Flexible thermoelectrics: From energy harvesting to human–machine interaction," J. Appl. Phys. **133**, 110901 (2023).

[12] N. Nischal Pillala and R. K. Dash, "Study of anisotropic thermal properties of GO/rGO based 1D Bi_2Te_3 thermoelectric nanomaterials for energy harvesting applications," AIP Conf. Proc. **2715**, 020005 (2023).

[13] R. A. Masut, "Heat transport in hot extruded bulk polycrystalline thermoelectric alloys based on Bi_2Te_3," J. Electron. Mater. **52**, 6929–6942 (2023).

[14] P. G. Klemens, "Thermal conductivity and lattice vibrational modes," in *Solid State Physics: Advances in Research and Applications*, edited by F. Seitz and D. Turnbull (Academic Press, Inc., New York, 1958), Vol. 7, pp. 1–70.

[15] J. Callaway, "Model for lattice thermal conductivity at low temperatures," Phys. Rev. **113**, 1046–1051 (1959).

[16] J. Callaway, "Low-temperature lattice thermal conductivity," Phys. Rev. **122**, 787–790 (1961).

[17] M. G. Holland, "Analysis of lattice thermal conductivity," Phys. Rev. **132**, 2461–2471 (1963).

[18] P. Carruthers, "Theory of thermal conductivity of solids at low temperatures," Rev. Mod. Phys. **33**, 92–138 (1961).

[19] B.-L. Huang and M. Kaviany, "*Ab initio* and molecular dynamics predictions for electron and phonon transport in bismuth telluride," Phys. Rev. B **77**, 125209 (2008).

[20] B. Qiu and X. L. Ruan, "Molecular dynamics simulations of lattice thermal conductivity of bismuth telluride using two-body interatomic potentials," Phys. Rev. B **80**, 165203 (2009).

[21] Y. Wang, B. Qiu, A. J. H. McGaughey, X. Ruan, and X. Xu, "Mode-wise thermal conductivity of bismuth telluride," J. Heat Transfer **135**, 091102 (2013).

[22] O. Hellman and D. A. Broido, "Phonon thermal transport in Bi_2Te_3 from first principles," Phys. Rev. B **90**, 134309 (2014).

[23] P. Al-Alam, G. Pernot, M. Isaiev, D. Lacroix, M. De Vos, N. Stein, D. Osenberg, and L. Philippe, "Lattice thermal conductivity of Bi_2Te_3 and SnSe using Debye-Callaway and Monte Carlo phonon transport modeling: Application to nanofilms and nanowires," Phys. Rev. B **100**, 115304 (2019).

[24] H. J. Goldsmid, "The thermal conductivity of bismuth telluride," Proc. Phys. Soc., Sect. B **69**, 203–209 (1956).

[25] H. J. Goldsmid, "Heat conduction in bismuth telluride," Proc. Phys. Soc. **72**, 17–26 (1958).

[26] C. B. Satterthwaite and R. W. Ure, Jr., "Electrical and thermal properties of Bi_2Te_3," Phys. Rev. **108**, 1164–1170 (1957).

[27] P. A. Walker, "The thermal conductivity and thermoelectric power of bismuth telluride at low temperatures," Proc. Phys. Soc. **76**, 113–126 (1960).

[28] H. Kaibe, Y. Tanaka, M. Sakata, and I. Nishida, "Anisotropic galvanomagnetic and thermoelectric properties of n-type Bi_2Te_3 single crystal with the composition of a useful thermoelectric cooling material," J. Phys. Chem. Solids **50**, 945–950 (1989).

[29] The c-Bi_2Te_3 lattice can be described as well by a primitive rhombohedral set of basic vectors, or by a conventional hexagonal unit cell which contains the rhombohedral cell; see for example Refs. 19 and 23.

[30] K. C. Lukas, W. S. Liu, G. Joshi, M. Zebarjadi, M. S. Dresselhaus, Z. F. Ren, G. Chen, and C. P. Opeil, "Experimental determination of the Lorenz number in $Cu_{0.01}Bi_2Te_{2.7}Se_{0.3}$ and $Bi_{0.88}Sb_{0.12}$," Phys. Rev. B **85**, 205410 (2012).

[31] M. Yao, M. Zebarjadi, and C. P. Opeil, "Experimental determination of phonon thermal conductivity and Lorenz ratio of single crystal metals: Al, Cu, and Zn," J. Appl. Phys. **122**, 135111 (2017).

[32] C.-H. Su, "Experimental determination of lattice thermal conductivity and Lorenz number as functions of temperature for n-type PbTe," Mater. Today Phys. **5**, 58–63 (2018).

[33] D. K. C. MacDonald, E. Moser, W. B. Pearson, I. M. Templeton, and S. B. Woods, "On the possibility of thermoelectric refrigeration at very low temperatures," Philos. Mag. **4**, 433–446 (1959).

[34] N. W. Ashcroft and N. D. Mermin, *Solid State Physics* (Saunders, Philadelphia, PA, 1976), Chap. 25, p. 501.

[35] H. J. Goldsmid, "Recent studies of bismuth telluride and its alloys," J. Appl. Phys. **32**, 2198–2202 (1961).

[36] J. Q. Jenkins, J. A. Rayne, and R. W. Ure, Jr., "Elastic moduli and phonon properties of Bi_2Te_3," Phys. Rev. B **5**, 3171–3184 (1972).

[37] J. Ma, W. Li, and X. Luo, "Examining the Callaway model for lattice thermal conductivity," Phys. Rev. B **90**, 035203 (2014).

[38] E. S. Itskevich, "The heat capacity of bismuth telluride at low temperatures," Sov. Phys. JETP **11**, 255–260 (1960).

[39]N. P. Gorbachuk, A. S. Bolgar, V. R. Sidorko, and L. V. Goncharuk, "Heat capacity and enthalpy of Bi_2Si_3 and Bi_2Te_3 in the temperature range 58-1012 K," Powder Metall. Met. Ceram. **43**, 284–290 (2004).
[40]Y. Sun, Y. Zhou, R. Gurunathan, J.-Y. Zhang, M. Hu, W. Liu, B. Xu, and G. J. Snyder, "Phonon scattering in the complex strain field of a dislocation in PbTe," J. Mater. Chem. C **9**, 8506–8514 (2021).
[41]Y. Zhang, "First-principles Debye-Callaway approach to lattice thermal conductivity," J. Materiomics **2**, 237–247 (2016).
[42]D. An, S. Chen, Z. Lu, R. Li, W. Chen, W. Fan, W. Wang, and Y. Wu, "Low thermal conductivity and optimized thermoelectric properties of p-type Te–Sb_2Se_3: Synergistic effect of doping and defect engineering," ACS Appl. Mater. Interfaces **11**, 27788–27797 (2019).
[43]F. Shi, H. Wang, Q. Zhang, X. Tan, Y. Yin, H. Hu, Z. Li, J. G. Noudem, G. Liu, and J. Jiang, "Improved thermoelectric properties of BiSbTe-$AgBiSe_2$ alloys by suppressing bipolar excitation," ACS Appl. Energy Mater. **4**, 2944–2950 (2021).